Coupled Sodium/Glucose Cotransport by SGLT1 Requires a Negative Charge at Position 454†

Ana Díez-Sampedro,‡,§ Donald D. F. Loo,§ Ernest M. Wright,§,|| Guido A. Zampighi,⊥ and Bruce A. Hirayama*,§

Departments of Physiology and Neurobiology, David Geffen School of Medicine at UCLA, 10833 Le Conte Avenue, Los Angeles, California 90095-1751

Received June 28, 2004; Revised Manuscript Received August 13, 2004

ABSTRACT: Na^+/glucose cotransport by SGLT1 is a tightly coupled process that is driven by the Na^+ electrochemical gradient across the plasma membrane. We have previously proposed that SGLT1 contains separate Na^+- and glucose-binding domains, that A166 (in the Na^+ domain) is close to D454 (in the sugar domain), and that interactions between these residues influence sugar specificity and transport. We have now expressed the mutant D454C in *Xenopus laevis* oocytes and examined the role of charge on residue 454 by replacing the Asp with Cys or His, and by chemical mutation of D454C with alkylating reagents of different charge ($MTSES^-$, $MTSET^+$, $MMTS^0$, $MTSHE^0$, and iodoacetate$^-$). Functional properties were examined by measuring sugar transport and cotransporter currents. In addition, D454C was labeled with fluorescent dyes and the fluorescence of the labeled transporter was recorded as a function of voltage and ligand concentration. The data shows that (1) aspartate 454 is critically important for the normal trafficking of the protein to the plasma membrane; (2) there were marked changes in the functional properties of D454C, i.e., a reduction in turnover number and a loss of voltage sensitivity, although there were no alterations in sugar selectivity or sugar and Na^+ affinity; (3) a negative charge on residue 454 increased Na^+ and sugar transport with a normal stoichiometry of 2 Na^+:1 sugar. A positive charge on residue 454, in contrast, uncoupled Na^+ and sugar transport, indicating the importance of the negative charge in the coordination of the cotransport mechanism.

Membrane cotransporters belong to a large class of ubiquitous proteins which convert the energy of the transmembrane electrochemical gradient into work to drive a cosubstrate across the membrane. They are found in all forms of life, from Archea to man, reflecting the importance of this basic process. Comparison of a large variety of unrelated cotransporters has revealed remarkable similarities in functional characteristics, indicating conservation of the basic mechanism among cotransporters with no primary amino acid sequence homology.

Arguably, the best functionally characterized example of a cotransporter is the mammalian Na^+/glucose cotransporter, SGLT1.[1] Studies have described transport kinetics, constructed kinetic models, and described the secondary structure of SGLT1, and details of the molecular motions involved continue to be discovered. The mechanism by which the process of cotransport is accomplished remains unknown. It is expected that insights into this process will be aided by studies following the recent determination of the atomic structure of the H^+/lactose permease (*1*).

SGLT1 has been shown to behave as if it is composed of two domains; Na^+ binding/translocation is located in the N-terminal part of the protein, and the C-terminal 5 transmembrane helices mediate sugar binding/translocation (e.g., refs *2*−*8*). Transport by SGLT1 is tightly coupled, with 2 Na^+ ions cotransported for each sugar molecule. This precise coordination requires that each domain relay the fact that its respective substrate is bound to the other domain. It is likely that this information is transmitted via conformational changes, but residues involved in the interaction between the domains have not been identified. Recently, a proposal was made that alanine 166, in the Na^+-binding domain, was functionally close to aspartate 454 in the sugar-binding domain (*9*). The charge at position 166 was found to be an important determinant in sugar transport.

In this study we have mutated residue 454 and investigated its functional consequences using biophysical and biochemical techniques. We find that the negative charge on this residue plays a major role in determining the stoichiometry of cotransport: If the charge at 454 is negative, the normal 2 Na:1 sugar stoichometry is maintained, but inserting a

† This work was supported by grants from the NIH (DK44602 and EY04410) and a Fellowship in Physiological Genomics from the American Physiological Society to A.D.-S.

* Correspondence: B. A. Hirayama; Department of Physiology, Geffen School of Medicine at UCLA, Los Angeles, CA 90095-1751; tel, 310-825-6968; fax, 310-206-5886; e-mail, bhirayama@mednet.ucla.edu.

‡ Current address: Department of Neurology, Yale Medical School, New Haven, CT 06520.

§ Department of Physiology.

|| Wright lab homepage: http://149.142.237.182/.

⊥ Department of Neurobiology.

[1] Abbreviations: SGLT1, Na^+/glucose cotransporter; MTS, methanethiosulfonate; $MTSES^-$, sodium(2-sulfonatoethyl)methanethiosulfonate; $MTSET^+$, 2-(trimethylammonium)ethyl methanethiosulfonate; $MTSHE^0$, (2-hydroxyethyl)methanethiosulfonate; $MMTS^0$, (methyl) methanethiosulfonate; TMR5M, tetramethylrhodamine-5-maleimide; TMR6M, tetramethylrhodamine-6-maleimide; αMDG, α-methyl-D-glucopyranoside; IMP, intramembrane particle; PepT1, H^+/dipeptide cotransporter; EAAC-1, Na^+/K^+/glutamate cotransporter; PutP, Na^+/proline cotransporter.

10.1021/bi048652d CCC: $27.50
Published on Web 09/25/2004

positive charge at this position uncouples Na^+ transport from sugar transport. Otherwise, the functional characteristics of D454C hSGLT1 were found to be similar to those of the wild-type protein.

MATERIALS AND METHODS

Oocytes. Stage V−VI oocytes from *Xenopus laevis* (Nasco, Fort Atkinson, WI) were injected with 50 ng of D454C mutant SGLT1 or wild-type cRNA and maintained at 18 °C for 3−7 days (*10*). Experiments were performed at 22 ± 1 °C.

Molecular Biology. Aspartic acid at the 454 position of human SGLT1 (hSGLT1) was replaced by cysteine (D454C) by site-directed mutagenesis using a two-step polymerase chain reaction protocol with the following oligonucleotide primers: D454C-sense, 5′-CAGCTCTTCTGTTACATC CAG-3′; and D454C-antisense, 5′-CTGGATGTAACAGAA-GAGCTG-3′. The underlined letters represent the mutation at amino acid position 454 to a cysteine, and a silent *Sap*I site was introduced as an aid in screening. The plasmid encoding wild-type hSGLT1 was used as template. PCR products were purified and combined in a final PCR reaction using the normal primers flanking the mutation site to produce an insert with *Avr*II and *Eco*47III restriction sites. The resulting fragment was ligated into a similarly treated wild-type hSGLT1-containing plasmid. Sequencing verified the presence of only the desired mutation. WT and D454C encoding plasmids were linearized with *Xba*I and transcribed (MEGA-script kit, Ambion, Austin, TX). The D454H mutant was constructed using the same procedure and the following primers: sense, 5′-CAG CTC TTC CAT TAC ATC CAG-3′; and antisense, 3′-GTC GAG AAG GTA ATG TAG GTC-5′, where the underlined letters represent the mutation to histidine and the silent *Sap*I restriction site. The double mutant, A166C/D454C was generated by standard protocols using the A166C (*9*) and D454C mutants.

Labeling the D454C Protein. D454C protein was labeled with cysteine-specific reagents in Na^+ buffer (100 mM NaCl, 2 mM KCl, 1 mM $CaCl_2$, 1 mM $MgCl_2$, and 10 mM HEPES, pH 7.5 with Tris) at 22 °C. Na^+ concentration in the buffer was varied by replacement with choline$^+$. The reagents used were $MTSET^+$ [2-(trimethylammonium)ethyl methanethiosulfonate], $MTSES^-$ [sodium(2-sulfonatoethyl)methanethiosulfonate], $MMTS^0$ [(methyl) methanethiosulfonate], $MTSHE^0$ [(2-hydroxyethyl)methanethiosulfonate] (Toronto Research Chemicals, Toronto, ON, Canada); tetramethylrhodamine-6-maleimide (TMR6M); and tetramethylrhodamine-5-maleimide (TMR5M) (Molecular Probes, Eugene, OR). Working concentrations of $MTSHE^0$ (1 mM) and $MMTS^0$ (1 mM) in Na^+ buffer were prepared from 100 mM stock solutions (in anhydrous dimethyl sulfoxide, kept frozen at −20 °C). $MTSES^-$ (1 mM) and $MTSET^+$ (1 mM) as well as the fluorophores (0.2 mM) were dissolved immediately before use. Iodoacetate was purchased from Sigma (St. Louis, MO), and labeling was in Na^+ buffer at pH 9 for 30 min.

Uptake Experiments. 50 μM substrate uptake into oocytes was measured using a radioactive tracer technique (*11*). ^{14}C-αMDG and ^{14}C-glucose were purchased from Amersham (Piscataway, NJ) or ICN (Costa Mesa, CA). The effect of labeling the 454 Cys was determined by pretreating the oocytes for 30 min at 22 °C in Na^+ buffer with 0.2−1 mM of the methanethiosulfonate reagent or fluorophore. The reactants were removed with two changes of choline buffer before exposure to the radioactive sugar.

Voltage-Clamp Experiments. The membrane potential was controlled and the currents were measured using the two-electrode voltage clamp (*12*). The D454C protein was labeled with a MTS reagent for 20−30 min and then washed with Na^+ buffer. The sugar-dependent current was the difference between the current recorded in the sugar and the previous record in Na^+ buffer alone. The experiments were controlled and data were acquired using pClamp software (Axon Instruments, Union City, CA). Although results from single oocytes are used to illustrate the data, all experiments were repeated on at least three oocytes from different donor frogs.

Stoichiometry Experiments. The charge to sugar transport stoichiometry was obtained by simultaneous measurement of sugar-induced current and sugar uptake (*13*, *14*). The oocytes were clamped at −100 mV. Charge transport was obtained as the difference between baseline and current in the presence of αMDG and was then integrated and converted to its molar equivalent of monovalent charge. [^{14}C]-αMDG uptake into noninjected oocytes was used as the control.

Fluorescence Experiments in the Voltage Clamp. D454C-expressing oocytes were labeled with TMR5M or TMR6M. Electrophysiological and fluorescence experiments were performed simultaneously (*15*). The membrane holding potential, V_h, was −50 mV, and currents in response to the voltage pulse protocol were measured using the two-electrode voltage clamp. Fluorescence intensity is expressed as arbitrary units (a.u.). The experiments were controlled using Clampex (pClamp7, Axon Instruments, Union City, CA). Examples of fluorescence records are from single oocytes; however, all experiments were repeated on at least 3 oocytes from different donor frogs.

Kinetics. To obtain the apparent Na^+ affinity ($K_{0.5}^{Na}$) of D454C the protein was labeled with TMR6M. The membrane voltage (V_m) was clamped at −50 mV, and the change in fluorescence (ΔF) was recorded as the V_m was jumped to +50 mV for 100 ms. Changes in ΔF at the end of the pulse were recorded as a function of Na^+ concentration. To estimate the apparent sugar affinities ($K_{0.5}^{sug}$) for D454C the protein was labeled with TMR5M and the membrane potential was stepped from −50 mV to −150 mV. The change in fluorescence (ΔF) was recorded as a function of sugar concentration. All the fluorescence data was corrected for photobleaching (*15*). The Na^+-induced or the sugar-induced increase in ΔF was plotted as a function of external concentration and fitted to the equation

$$\Delta F = \Delta F_{max} S^n/(S^n + (K_{0.5})^n) \quad (1)$$

where ΔF_{max} is the maximal change in fluorescence, S is substrate concentration, $K_{0.5}$ is the substrate concentration for $0.5\Delta F_{max}$, and n is the Hill coefficient. For sugar kinetics $n = 1$.

Pre-Steady-State Charge. The pre-steady-state transient charge Q was determined by using the fitted method (*12*). The charge was calculated by integration of this transient current with time, and the distribution of the charge moved as a function of membrane voltage (V) was calculated by fitting the data with the Boltzmann relationship:

$$(Q - Q_{hyp})/Q_{max} = 1/\{1 + \exp[z(V - V_{0.5})F/RT]\} \quad (2)$$

where $Q_{max} = Q_{dep} - Q_{hyp}$ (Q_{dep} and Q_{hyp} are Q at depolarizing and hyperpolarizing limits, respectively), F is the Faraday constant, R is the gas constant, T is the absolute temperature, $V_{0.5}^{Q}$ is the membrane potential where there is 50% charge transfer, and z is the apparent valence of the movable charge. The Boltzmann relation was also used to fit the dependence of change of fluorescence intensity (ΔF) on membrane voltage (ΔF vs V), where $V_{0.5}^{F}$ and ΔF_{max} are the corresponding values for fluorescence. Fits of data with equations were performed using Sigmaplot 2000 (SPSS, Chicago, IL).

Time Constant. Time constants (τ) for charge movement were estimated by fitting the data to two exponentials, membrane capacitance and transporter pre-steady-state charge (*12*). The τ for ΔF was estimated from a fit to one exponential (*16*). SigmaPlot (ver. 8.0, SPSS) and Clampfit (ver. 8.1, Axon Instruments) were used for the fits.

Freeze−Fracture Electron Microscopy. Visual determination of protein expression in the oocyte plasma membrane was done as in ref *17*. Functional expression was estimated for each oocyte from measurement of Q_{max}.

RESULTS

Functional Characterization of the Mutant D454C. Sugar Uptake. Measurements of sugar uptake (50 μM sugar for 30 min) were done in noninjected oocytes, oocytes expressing the wild-type protein, hSGLT1, or oocytes expressing the mutant D454C (Figure 1). The sugar uptake in the mutant (3.3 ± 0.2 pmol/30 min) was low compared with the uptake in the wild-type protein (125 ± 20 pmol/30 min), but significantly higher than in the noninjected oocytes (0.5 ± 0.02 pmol/30 min). Uptake in D454H was 10 ± 1 pmol/30 min ($n = 3$, not shown), and expression of the double mutant A166C/D454C was not measurable.

Electrophysiology. Charge Movements. D454C displayed pre-steady-state charge movements and substrate-dependent steady-state currents. Although the expression of the D454C mutant was low, our measurements showed that pre-steady-state charge movements in D454C had properties similar to those of the wild-type hSGLT1 (*12*). Oocytes expressing the D454C hSGLT1 were clamped at −50 mV. Figure 2 shows the Na^+-dependent pre-steady-state current. When the potential was jumped to a new value in the presence of Na^+ (A, C), an initial membrane capacitive transient with a time constant (τ) of ~1 ms was generated, and this was followed by a slower transporter transient (ON) ($\tau = 4-20$ ms) before the current reached a steady-state value. Upon returning to the holding potential ($V_h = -50$mV) there was an initial fast capacitive transient due to the membrane capacitance followed by a slower transporter current (OFF) that decayed with a τ of ~15 ms (Figure 2). This slow transient current was not observed in the absence of Na^+. Only the membrane capacitive transients were observed in control oocytes.

The ON and the OFF transporter currents were isolated and integrated to obtain the amount of transporter charge moved (Q) after each voltage step. Q was plotted against voltage and fit to the Boltzmann equation to obtain the maximal charge moved (Q_{max}), the apparent valence of the movable charge (z), and the voltage at which 50% of the charge is moved ($V_{0.5}^{Q}$, see Materials and Methods and Figure 3). Although Q_{max} for the D454C oocyte was small compared with the oocyte expressing the wild-type transporter (e.g., 0.9 nC vs 16 nC, in representative oocytes from one batch, Figure 3), we could clearly detect functional effects of substrate on pre-steady-state charge distribution. The addition of 100 mM αMDG to the bath solution shifted the $V_{0.5}$ to more positive voltages (not shown), whereas for the wild-type protein Q was reduced (*12*). $V_{0.5}^{Q}$ was ~−20 to −30 mV for D454C in the absence of sugar (Figure 3A) and ~+10 mV in the presence of sugar (not shown). $V_{0.5}^{Q}$ was −47 mV for wild-type hSGLT1 in the absence of sugar (Figure 3B).

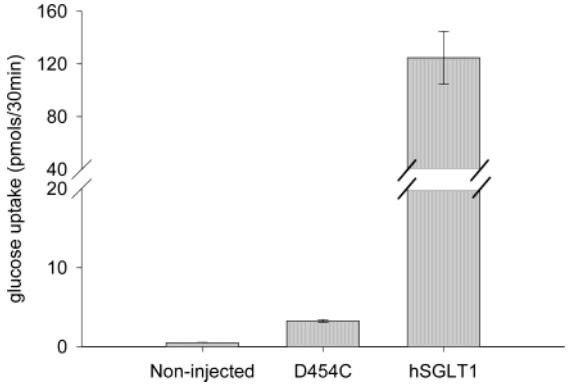

FIGURE 1: 50 μM glucose uptake (30 min) in noninjected oocytes, in oocytes expressing the mutant D454C, and in oocytes expressing the wild-type hSGLT1. Uptakes are the mean of 8−12 oocytes and are expressed as the mean ± SEM.

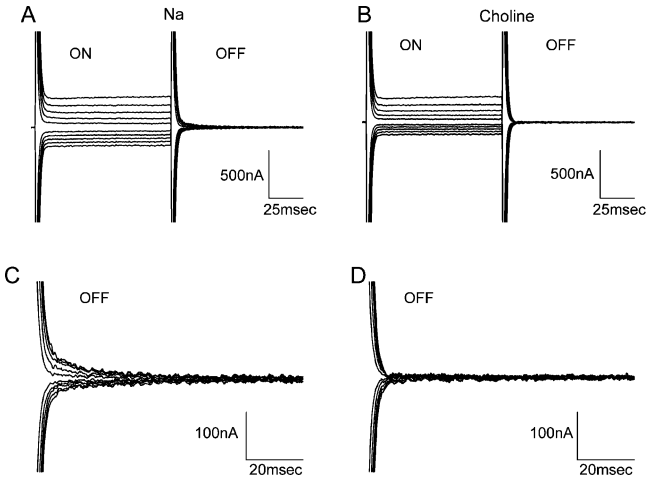

FIGURE 2: Current records from a single oocyte expressing D454C. The membrane voltage was initially held at −50 mV and then jumped from −50 mV to different voltages (ranging from +50 to −150 mV in 20 mV decrements). Each new voltage was applied for 100 ms ("ON") and then returned to the holding voltage for another 100 ms ("OFF"). Records are shown in the presence (A, C) and absence of Na^+ (B, D). The pre-steady-state transient was generated in the presence of Na^+. Panels C and D are magnified views of the records as the membrane potential was returned to the holding potential to more clearly show the characteristics of the Na^+-dependent pre-steady-state current. The records are offset to zero for clarity.

The functional data suggested that there was low expression of the mutant protein in the plasma membrane of the oocyte compared to wild-type hSGLT1. This was confirmed by the number of intramembrane particles in the plasma membrane of the oocyte (Figure 4). The density of particles

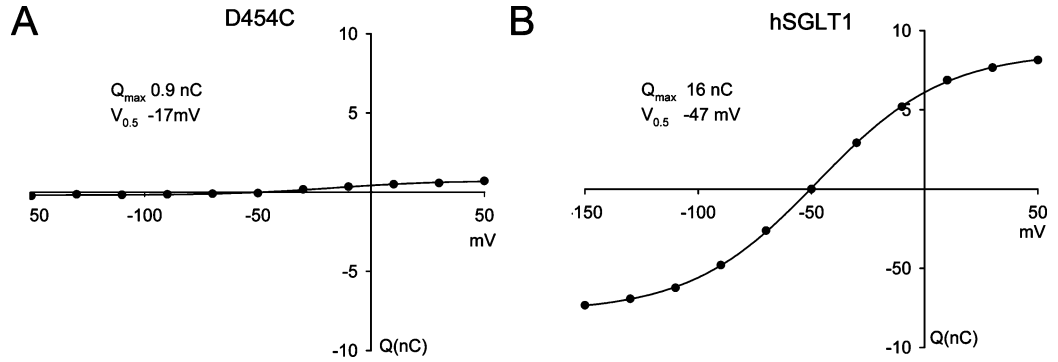

FIGURE 3: The charge−voltage (Q/V) curves of wild-type and D454C SGLT1 oocytes with membrane voltage varying from +50 to −150 mV. (A) Charge movement in a D454C expressing oocyte. The solid line was the fit of the data to the Boltzmann equation (Q_{max}, 3 ± 0.5 nC; $V_{0.5}^{Q}$, −20 ± 5 mV; z, 1 ± 0.2). (B) A hSGLT1 oocyte. The Boltzmann parameters were Q_{max}, 16.4 ± 0.1 nC; $V_{0.5}^{Q}$, −47 ± 0.4 mV; z, 0.9 ± 0.1.

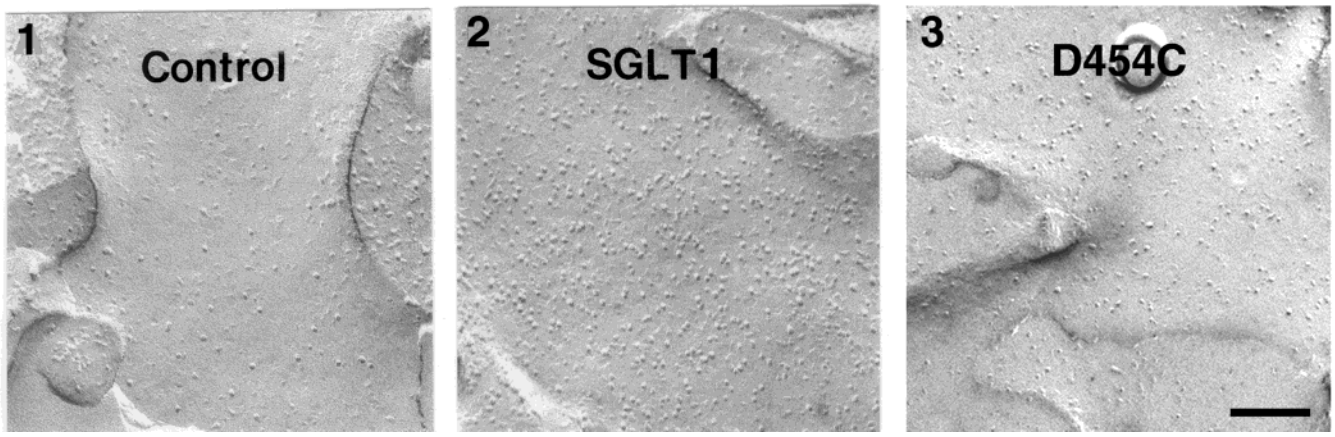

FIGURE 4: Freeze−fracture electron microscopy of the plasma membrane of a D454C-expressing oocyte (3) (the same oocytes shown in Figure 5), one expressing hSGLT1 (2), and a noninjected oocyte (1). In the D454C oocytes there were 500 particles/μm^2, 3200 in the hSGLT1 oocyte, and 300 in the noninjected oocyte. The total area of the plasma membrane was estimated from the capacitance of the D454C oocytes (24×10^6 μm^2). Scale bar is 100 nm.

in noninjected oocytes was ∼200/μm^2. This density increased to ∼500/μm^2 in oocytes expressing D454C. In contrast, the density of the SGLT1 wild-type protein particles was much higher (∼ 3200/μm^2) (see also ref *17*), indicating that the mutant protein expression was significantly higher than the expression in noninjected controls, but less than 10% that of the wild-type.

Fluorescence of TMR5M- and TMR6M-Labeled D454C. Oocytes expressing D454C were labeled with TMR5M or TMR6M. There was a change in fluorescence intensity (ΔF) in response to the voltage pulse protocol. In Na^+ (Figure 5A), for depolarizing voltages the fluorescence of D454C TMR5M increased while at hyperpolarizing voltages ΔF decreased. When sugar was added to the medium (Figure 5C), ΔF decreased at both hyper- and depolarizing voltages, but was most pronounced in response to negative voltages. In the absence of Na^+ (Figure 5B), the record was similar to the one in Na^+, but ΔF was smaller. In 0.2 mM phlorizin (Figure 5D) the fluorescence was further decreased. $V_{0.5}^{F}$ (the voltage at which ΔF is $0.5\Delta F_{max}$) was calculated by fitting the $\Delta F/V$ curve to the Boltzmann equation. In Na^+, $V_{0.5}^{F}$ was −35 mV and z was 0.6 (Figure 6A). When 100 mM αMDG was added, $V_{0.5}^{F}$ became more positive, but it is difficult to estimate the value since the $\Delta F/V$ curve did not saturate at positive values (not shown). In neither the absence of Na^+ nor the presence of phlorizin (Pz) was the ΔF saturable with voltage at either hyperpolarizing or depolarizing voltages.

The time constants for the fluorescence changes (τ) were also calculated. In the presence and in the absence of Na^+ (Figure 5A,B) the τ values were ∼18 ms, independent of voltage. When sugar was present (Figure 5C), τ was slower for depolarizing (24 ms) than for hyperpolarizing voltages (8 ms). In phlorizin (Figure 5D) τ was greater (41 ms) at hyperpolarizing than at depolarizing potentials (27 ms).

The polarities of the fluorescence response depended on the isomer of the dye conjugated to residue 454C. With the 6-isomer (TMR6M) in Na^+ the ΔF decreased at depolarizing voltages and increased at hyperpolarizing voltages (Figure 7A). When 100 mM αMDG was present (Figure 7C), the ΔF were larger at depolarizing voltages. If Na^+ was removed (Figure 7B), the ΔF were smaller. Phlorizin (Figure 7D) almost abolished the fluorescence response. In Na^+, $V_{0.5}^{F}$ was −37 mV and z was 0.7 (Figure 6B) as for TMR5M D454C. Adding sugar shifted the $V_{0.5}^{F}$ to more positive values (−15 mV), and on removal of external Na^+, the $V_{0.5}^{F}$ shifted to more negative values (see Figure 9). In all the conditions, τ was slower for depolarizing voltages than for hyperpolarizing voltages and in sugar did not reach a steady state at 100 ms (Figure 7C).

Na^+ and Sugar Kinetics of the D454C Mutant. The kinetic characterization of the mutant was done by labeling the

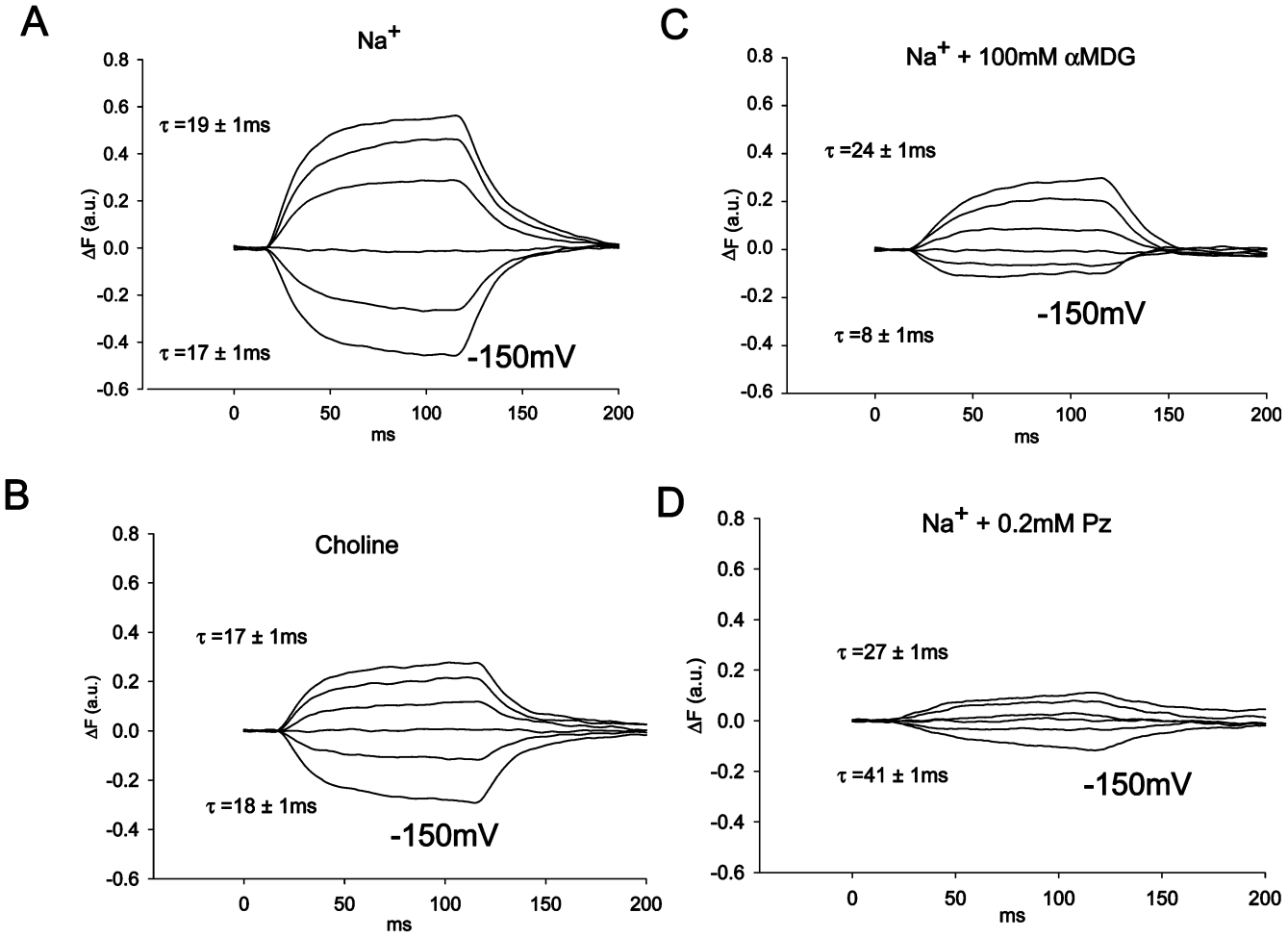

FIGURE 5: Voltage-induced fluorescence changes of TMR5M-labeled D454C. The oocyte was clamped at −50 mV, and the membrane voltage was stepped from −150 mV to +50 mV for 100 ms in the presence and absence of Na^+ (A, B), 100 mM sugar (C), and 0.2 mM phlorizin (D). Traces are shown for +50, +30, −10, −50, −90, and −150 mV.

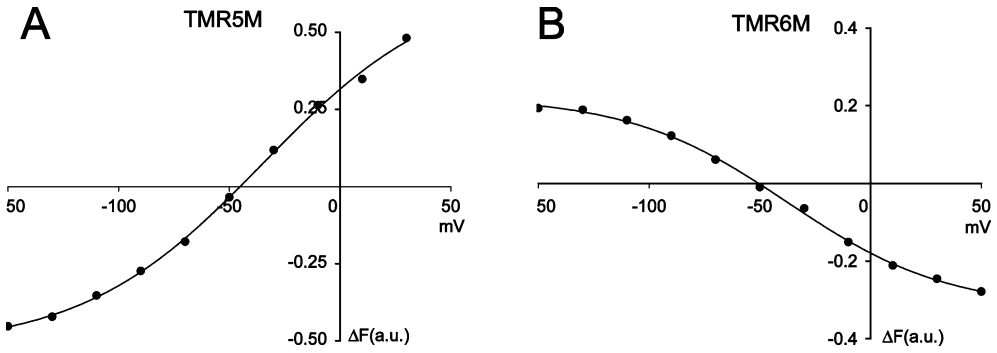

FIGURE 6: TMRM fluorescence as a function of voltage ($\Delta F/V$) in D454C-expressing oocytes treated with TMR5M (A) or TMR6M (B) with 100 ms pulses. The data were fitted with eq 2. The $V_{0.5}{}^F$ values (median voltage of the $\Delta F/V$ relation) are −35 ± 4 mV and −37 ± 2 mV, respectively, and the z values are 0.6 ± 0.1 and 0.7 ± 0.1.

protein with the TMRM dyes and using substrate-dependent changes in ΔF to determine the kinetics of the mutant transporter (*15*).

Apparent Na^+ Affinity, $K_{0.5}{}^{Na}$. D454C was labeled with TMR6M, and changes in fluorescence were recorded at 0−100 mM NaCl. Fitting the data with eq 1 indicated that the $K_{0.5}{}^{Na}$ was 12 ± 1mM and the Hill coefficient (n) was 1.5 (Figure 8). In 3 different oocytes $K_{0.5}{}^{Na}$ was 10 ± 2 mM and n was 2 ± 0.5.

Figure 9 shows a semilog plot of $V_{0.5}{}^F$ as a function of Na^+ concentration (the inset represents ΔF as a function of voltage at 25 mM Na^+). The slope was 50 mV per 10-fold change in [Na], and $V_{0.5}{}^F$ at <1 mM Na^+ is extrapolated to be ∼−120 mV.

Apparent Sugar Affinities: αMDG and Glucose. The protein was labeled with TMR5M, and the αMDG and glucose $K_{0.5}$'s were obtained by recording ΔF as a function of the sugar concentration. The apparent D-glucose and αMDG affinities were 0.7 ± 0.1 mM and 0.6 ± 0.1 mM (Figure 10).

Role of Charge at Position 454. We investigated the influence of charge at position 454 with negatively charged ($MTSES^-$ or $iodoacetate^-$), positive ($MTSET^+$), or neutral

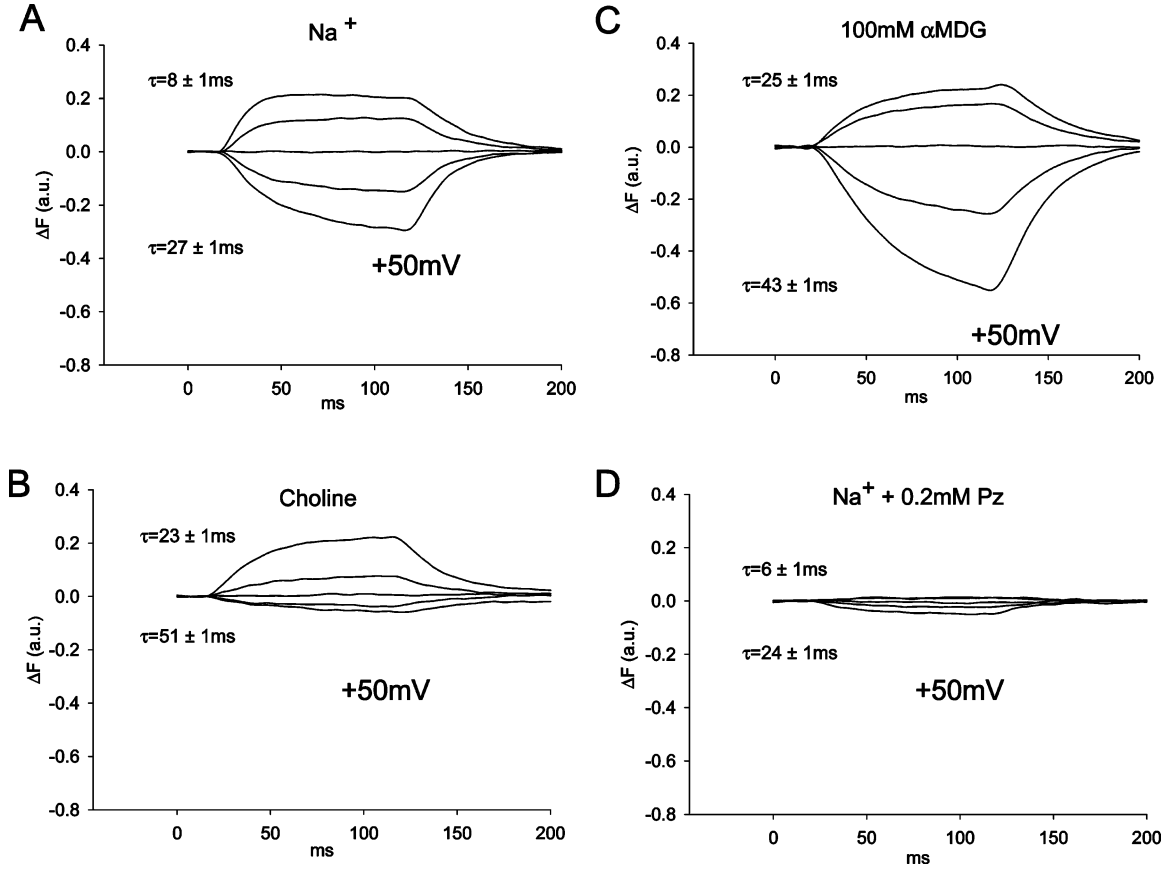

FIGURE 7: Voltage-induced fluorescence changes of TMR6M-labeled D454C. The oocyte was clamped at −50 mV, and the membrane voltage was stepped from −150 mV to +50 mV for 100 ms in the presence and absence of Na (A, B), 100 mM sugar (C), and 0.2 mM phlorizin (D). Traces are shown for +50, −10, −50, −90, and −150 mV.

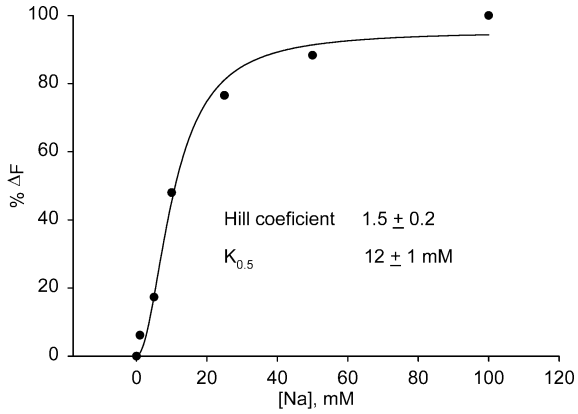

FIGURE 8: Effect of Na^+ concentration on D454C TMR6M fluorescence. At each Na concentration the fluorescence change (ΔF) resulting from a voltage jump from −50 mV to +50 mV was plotted against Na^+ concentration. The data were corrected for photobleaching and fitted to eq 1. The Hill coefficient was 1.5 ± 0.2.

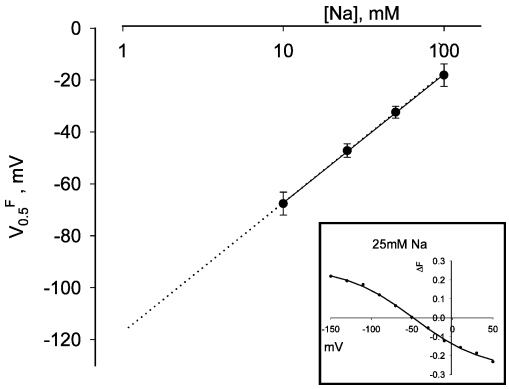

FIGURE 9: Apparent affinity for Na^+ obtained using TMR6M fluorescence. The effect of Na^+ concentration in the distribution of the protein is represented by $V_{0.5}{}^F$. $V_{0.5}{}^F$ was measured at each concentration of Na^+, and was calculated from the $\Delta F/V$ curve (the inset shows the $\Delta F/V$ curve obtained at 25 mM Na^+).

(MMTS^0, MTSHE^0) cysteine-specific reagents, and by mutating D454 to histidine.

Uptake of Sugar. αMDG uptake increased 2.5 times (Figure 11A; $p < 0.0001$) when the protein was labeled with $MTSES^-$ compared to the unlabeled control. There was no change in sugar uptake with $MTSET^+$. Glucose uptake (Figure 11B) was also increased by $MTSES^-$ but not by $MTSET^+$. There was no significant difference in uptake after labeling with either MMTS^0 or MTSHE^0 (not shown). In noninjected or in hSGLT1 oocytes αMDG and glucose uptakes were unaffected by any MTS reagent or iodoacetate$^-$.

Substrate-Dependent Currents. Figure 12 shows the $I-V$ curve of the sugar-induced current in a D454C expressing oocyte. The glucose- and αMDG-induced currents were small (<30 nA) and voltage-independent from 0 to −150 mV. After labeling with $MTSES^-$, the αMDG-induced current increased (Figure 12A) and remained voltage-independent. In contrast, after labeling with $MTSET^+$ (Figure 12B) the glucose-induced current became voltage-dependent and did not saturate at the largest hyperpolarizing potential (−150 mV). At positive potentials the glucose-induced current of the $MTSET^+$-labeled D454C was inhibited. The effect of charged MTS reagents on voltage-dependence of

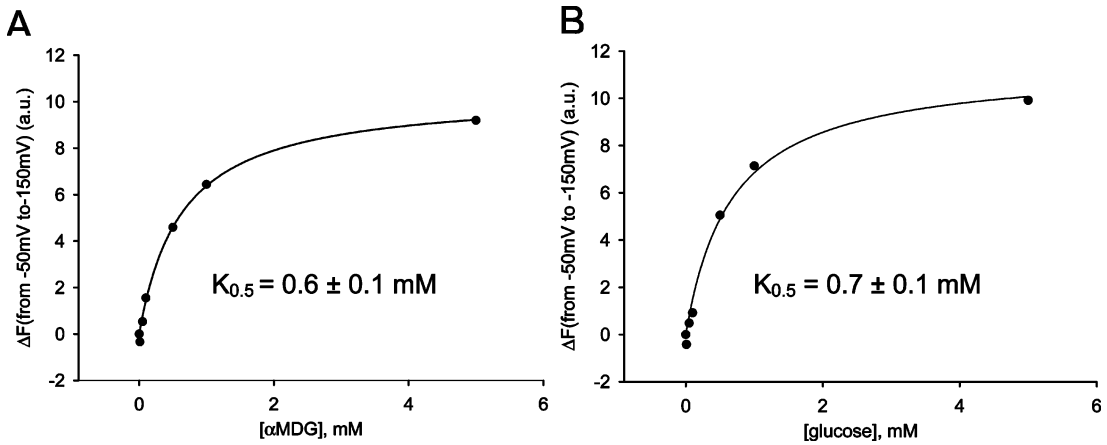

FIGURE 10: Apparent affinity for glucose and αMDG obtained using TMR5M fluorescence. Changes in fluorescence were measured as ΔF plotted against the αMDG concentration (A) or the D-glucose concentration (B) when the membrane voltage was jumped from −50 mV to −150 mV at different sugar concentrations. Similar results were obtained in four different experiments. The experiments were repeated five times, yielding similar results (0.6 ± 0.1 mM and 0.5 ± 0.1 mM). Data was corrected for photobleaching.

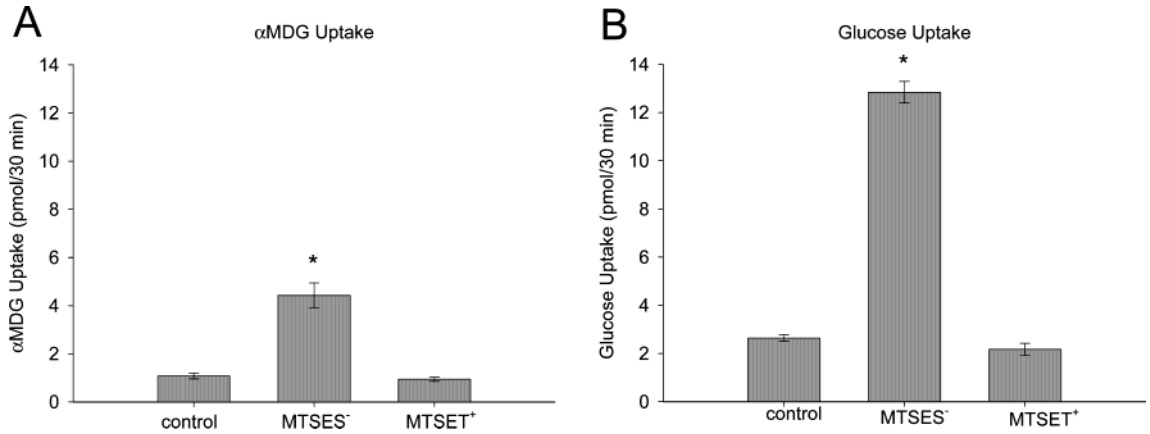

FIGURE 11: (A) Effect of 1 mM $MTSES^-$ or 1 mM $MTSET^+$ on 50 μM αMDG uptakes in 9−12 oocytes expressing D454C and (B) on 50 μM D-glucose uptakes. Background uptake from noninjected oocytes otherwise treated identically was subtracted. (*) Significantly different from control ($P < 0.00001$).

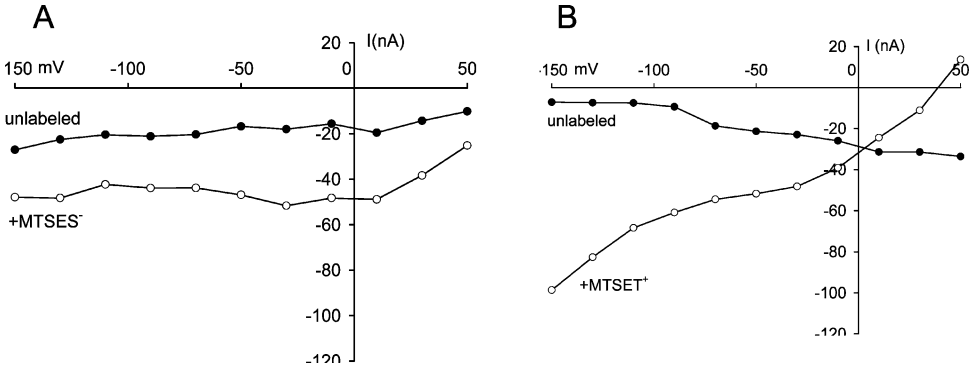

FIGURE 12: Current−voltage ($I-V$) curves in D454C-expressing oocytes. Effect of labeling the protein with 1 mM $MTSES^-$ or 1 mM $MTSET^+$ on the sugar-induced current. (A) 150 mM αMDG-induced current in an oocyte expressing D454C before and after incubation in $MTSES^-$. (B) 150 mM glucose-induced current in an oocyte expressing D454C before and after labeling the protein with $MTSET^+$.

the sugar-induced current was independent of the identity of the sugar. We did not observe any effect of the charge of MTS reagents on either the pre-steady-state current or the uncoupled steady-state current in the absence of sugar.

D454C Stoichiometry: Ratio of Charge Uptake/αMDG Uptake. We simultaneously measured sugar uptake and sugar-induced current in D454C oocytes treated with $MTSES^-$ and $MTSET^+$. The current was recorded for 5 min after 2 mM αMDG (+ ^{14}C-αMDG) was added to the medium. The sugar-induced current was integrated and converted to picomoles of positive charge and compared with sugar uptake. The ratios were ∼2 positive charges:1 sugar for the $MTSES^-$-labeled oocytes and ∼5 positive charges:1 sugar for $MTSET^+$-labeled D454C (Figure 13). The small sugar-induced current in the unlabeled D454C precluded a reliable estimate of stoichiometry.

DISCUSSION

Ion-driven cotransporters are molecular machines which are able to convert the transmembrane electrochemical

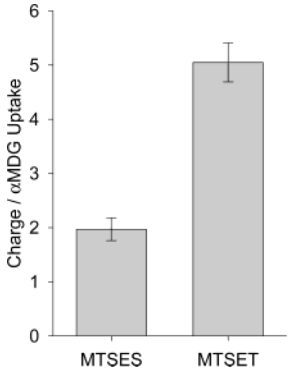

FIGURE 13: Effect of 1 mM $MTSES^-$ or 1 mM $MTSET^+$ on the ratio of inward positive charge/αMDG uptake in oocytes expressing D454C. Oocytes were incubated with one of the reagents for 20−40 min, and 2 mM αMDG uptake and inward charge were measured simultaneously for 5 min in each oocyte expressing D454C. The inward charge and sugar uptake was calculated as described in Materials and Methods. The charge:sugar uptake ratio was determined for each oocyte. Charge uptake after $MTSES^-$ ranged from 62 to 130 pmol, sugar uptake from 34 to 59 pmol, and charge:sugar stoichiometry = 2.0 ± 0.2 (SEM, n = 5); for $MTSET^+$ positive charge uptake ranged from 103 to 157 pmol and sugar uptake was from 18 to 29 pmol, and the stoichiometry = 5.0 ± 0.4 (n = 4).

gradient into physical work, i.e., energy from transport of the cation down its gradient enables driving the cosubstrate across the cell membrane, potentially against its concentration gradient. Similarity of the functional characteristics of cotransporters from unrelated gene families suggests a conservation of the basic mechanism. Previous studies on SGLT1 by several groups (e.g., refs *10*, *16*, *18*, *19*) indicate that binding on the external face of the transporter is ordered, with Na^+ binding first. Na^+ binding, in the N-terminal part of SGLT1 (e.g., refs *2*, *3*, *5*, *6*, *9*), initiates a conformational change that results in an increase in the affinity for sugar in the C-terminal domain (e.g., refs *7*, *8*). Sugar binding then induces another series of conformational changes that results in transport (*15*, *16*), i.e., reorientation of the Na^+- and sugar-binding sites to face the cytoplasm. The residues involved in this interdomain coordination have not been identified.

Recent experiments indicated that residue 166 in the Na^+ domain is close enough to affect, or is directly involved in, an interaction with residues in the sugar domain which altered sugar-binding specificity (*9*). As inhibition of transport was dependent on the presence of a positive charge at 166, we speculated that a potential candidate for this inhibitory interaction was the aspartic acid at position 454 because cross-linking studies suggested that these residues were in close proximity (*20*). In this study we functionally characterize the D454C mutant human SGLT1 using a variety of biochemical and biophysical methods, and describe the functional consequences of charge at this location.

Characterization of the D454C Mutant. D454C has low expression compared to the wild-type hSGLT1 protein. The ^{14}C-sugar uptake and currents indicated that the functional expression was less than 2% of wild-type (Figures 1, 12) while Q_{max} (*12*) and freeze−fracture electron microscopy measurements (*17*) indicated that D454C protein density in the plasma membrane was less than 10% compared with wild-type protein (Figures 3, 4). The apparent discrepancy between functional level and protein expression is explained, at least in part, by the low turnover of D454C ($MTSES^-$ treatment increased the sugar uptake and current by ∼2.5-fold, Figure 11). The low density in the plasma membrane suggests that the residue at the 454 position was important for the trafficking of the protein to the plasma membrane, as noted for many other SGLT1 mutants (*21*). The functional expression of D454H was also only ∼10% of WT (not shown), and the double mutant A166C/D454C was functionally inactive.

The low expression made characterization of the D454C mutant difficult using radioactive tracer uptake and electrophysiology. We took advantage of our ability to attach a fluorescent probe to the 454C residue, and used voltage-induced and substrate-induced conformational changes reported by the fluorescent probe to measure the apparent kinetics of Na^+ and sugar binding (*15*). The 454C residue is predicted to be in an external loop between transmembrane helices 10 and 11 (*4*), and it is accessible to large cysteine-specific reagents. When D454C was labeled with TMR6M (Figure 7), the voltage-induced fluorescence changes (ΔF) were similar to those of Q457C labeled with this dye (*15*, *16*): Hyperpolarization of the membrane caused an increase in ΔF with a time constant of 6 ± 1 ms (n = 3), while depolarization decreased ΔF with a time constant of 31 ± 1 ms (n = 3). The magnitude of ΔF was ligand-dependent, and phlorizin blocked the fluorescence changes (Figure 7). This similarity in the fluorescence response indicates that the closely spaced residues 454 and 457 experience similar environmental changes as substrates, inhibitors, and voltage modify the conformation of the protein. We note with interest that the shift in $V_{0.5}^F$ for a 10-fold reduction in $[Na^+]$ for D454C labeled with TMR6M was −50 mV, whereas for Q457C it is −100 mV.

When 454C was labeled with TMR5M, changes in the fluorescence were similar to those for TMR6M (Figure 5), but the polarity of ΔF in response to voltage was inverted so that hyperpolarizing decreased ΔF (τ = 19 ± 1 ms, n = 5), depolarizing voltage increased ΔF (τ = 12 ± 1, n = 5), and sugar decreased ΔF. The inversion in fluorescence polarity with voltage between the 5- and 6-isomers indicates that the fluorescent moiety experiences different environments due to the small positional difference imposed by the molecular geometry.

The apparent affinity for Na^+ ($K_{0.5}^{Na}$) was obtained from the Na^+ dependence of TMR6M ΔF. We observed a sigmoidal increase in ΔF with increasing $[Na^+]$ with a $K_{0.5}^{Na}$ of 12 mM and a Hill coefficient of 1.5 (Figure 8). Similarly, when 454C was labeled with TMR5M, in the presence of 100 mM Na^+, we observed a hyperbolic concentration-dependent decrease in ΔF as the [sugar] increased with a $K_{0.5}^{sugar}$ for glucose and αMDG of 0.6 mM (Figure 10). This is similar to that for Q457C (*15*, *16*). Both $K_{0.5}$ values, for Na^+ and sugar, were unchanged from the value for the wild-type protein (*22*), indicating that the substitution of the aspartate for a cysteine at the 454 residue was not important for the affinity of either substrate, and suggesting that the 454 residue does not form a part of either the sugar- or Na^+-binding sites. In contrast, residue 457 directly interacts with the sugar, and modifications to this position adversely affect the $K_{0.5}^{sugar}$ and/or transport (*7*).

Role of 454 in Cotransport. Perhaps most significantly, residue 454 has a critical role in the transport mechanism.

In the SGLT1 wild-type protein the cosubstrate coupling stoichiometry is very strict: 2 Na^+ are transported for each sugar (*6*, *13*, *23*). The stoichiometry after labeling D454C with $MTSES^-$ was 2 Na^+:1 sugar (we project that the charge is a Na^+ ion, as sugar uptake was Na^+-dependent). Labeling D454C with $MTSET^+$ increased the coupling ratio to 5. Glucose uptake was consistently higher than αMDG uptake, whereas there was no difference in $K_{0.5}^{sug}$, suggesting that an interaction by the α-methyl group with elements in the sugar transport pathway decreased turnover rate. In two D454H oocytes the stoichiometry for uptake at pH 7.5 was 2 Na^+:1 sugar, but when the experiment was done at pH 5.0 (three oocytes) the stoichiometry was 3 Na^+:1 sugar (not shown). Although the actual pK_a of histidine in the protein is not known, the free solution pK_a of histidine is 6.0, a result consistent with the protonation of this histidine resulting in uncoupling of transport. This suggests that the charge at position 454 plays an important role in coupling Na^+ and sugar uptake.

The charge at position 454 influenced the voltage dependence of transport. In the wild-type transporter the sugar-induced current increases as the voltage becomes more negative and saturates as V_m reaches about −150 mV (e.g., refs *6*, *22*, *24*, *25*). In D454C the voltage-dependence of the sugar-dependent current was shifted to positive potentials compared to the wild-type and was voltage-independent for negative values of V_m (Figure 12). This is consistent with the $V_{0.5}^Q$ shift of the pre-steady-state current (not shown). Producing a negatively charged residue at position 454, by labeling the protein with $MTSES^-$, increased sugar uptake (Figure 11) and sugar-dependent current with no change in voltage sensitivity (Figure 12A). A similar increase in uptake was observed after labeling with $iodoacetate^-$ (not shown). In contrast, if D454C was labeled with $MTSET^+$, a positively charged reagent, sugar transport was unchanged but uncoupled from Na^+ (Figures 11 and 13). The sugar-induced current was voltage sensitive from +50 to −150 mV, twice as large at −150 mV as for the $MTSES^-$-labeled condition, and reversed at about +40 mV (Figure 12B). These effects of charge at position 454 were sugar-dependent: we could not detect any change in the magnitude or voltage-dependence of the uncoupled current in the absence of sugar.

In A166C there were also differences in maximal transport rate (I_{max}) as well as $K_{0.5}^{sug}$. Both D-glucose and D-galactose had higher I_{max} values than αMDG, but the $K_{0.5}^{sug}$ values of αMDG and D-glucose were identical, and about 3-fold higher than that of D-galactose. This was attributed to an alteration in the sugar-binding site as a structural response to the change in a residue adjacent to the binding site (*9*). For D454C there is no difference between the sugars in $K_{0.5}^{sug}$.

The importance of a charged residue adjacent to the substrate-binding site may be part of a general theme for coupling cosubstrate transport. Our results in hSGLT1 show a structural and functional parallel to the glutamate transporter (EAAC-1). Borre and Kanner (*26*) neutralized the positively charged arginine 445 of EAAC-1 by substitution with serine (R445S), and created a glutamate-gated cation conductance which is dependent on the structure of the bound substrate. Significantly, this site is only 2 residues from arginine 447, which is proposed to bind to the γ-carboxyl group of glutamate in the binding site (*27*). In hSGLT1 D454 is only 3 residues from glutamine 457, which appears to interact with O1 and O5 of the sugar in the binding and translocation pathway (*7*). In contrast to EAAC-1, however, it does not appear that 454 has a direct influence on substrate binding, since we observed no alterations in the apparent kinetics of ion or sugar binding from the wild-type.

The role of charged residues in coupling has been shown in several other bacterial and eucaryotic transporters. Mutation of the conserved arginine 282 to glutamate in the rabbit H^+-dipeptide cotransporter (PepT1) uncoupled the mechanism so that dipeptides were transported down their concentration gradient, and dipeptide binding opened a H^+ conductance, with little effect on kinetics (*28*), and in hSGLT1, mutation of aspartate 204 (proposed to face the cytoplasm) to asparagine (D204N) produced a glucose-gated H^+ channel (*6*). In bacteria glutamate 269 of the lactose permease is involved in substrate−cation coupling, and the crystal structure shows that the substrate homologue β-D-galactopyranosyl-1-thio-β-D-galactopyranoside interacts with two residues, arginine 144 and tryptophan 151, involved in substrate binding (*1*). The residue arginine 40 of the Na^+/proline cotransporter (PutP) is involved in cation specificity, and alkylation of the cysteine mutant (R40C) uncouples proline transport (*29*).

Although we have shown that the negative charge at 454 is essential for coupling Na^+ glucose cotransport, it does not appear to be the sole arbiter. Sequence comparison of SGLT isoforms 1, 2, and 3 from several species places a negatively charged residue here for 1 and 2, which are sugar transporters, but a His in hSGLT3, which is a sugar sensor, and cannot transport sugar (*23*). Simply changing residue 454 from Asp to His does not reproduce the SGLT3 phenotype: D454H SGLT1 transports sugar. For all of the isoforms, residue 166 is an alanine (*4*). So, although 166 and 454 are thought to be physically close together in at least some conformational states of SGLT1, and the charge of residue 166 influences the conformation of the sugar-binding site, coupling is probably not mediated by a direct interaction between them. We suspect that a charged or polar residue in another loop may interact with 454 and also be critical in stoichiometry.

In conclusion, these observations suggest that the negative charge at position 454 is intimately involved in a specific part of the mechanism of cotransport. (1) Na^+ binds to the transporter irrespective of the charge on residue 454; (2) as in the wild-type, sugar binding requires Na^+ to be bound, and binding is charge independent; (3) after sugar binds, it can be transported by the protein; and (4) after sugar binds, Na^+ can be transported; but (5) only if the charge at residue 454 is negative are Na^+ and sugar cotransported together with the wild-type stoichiometry of 2 Na^+:1 sugar. We therefore suggest that the primary role of residue 454 is to coordinate the function of the Na^+ and sugar domains, which results in stoichiometric cotransport.

ACKNOWLEDGMENT

We thank Mr. Michael Kreman for the freeze−fracture electron microscopy, Ms. Amanda Johnson and Ms. Kari Edwards for technical assistance with the oocytes, and Dr. Eric Turk for help in designing the mutations.

REFERENCES

1. Abramson, J., Smirnova, I., Kasho, V., Verner, G., Kaback, H. R., and Iwata, S. (2003) Structure and mechanism of the lactose permease of *Escherichia coli*. *Science 301*, 610−615.

2. Panayotova-Heiermann, M., Loo, D. D. F., Kong, C.-T., Lever, J. E., and Wright, E. M. (1996) Sugar binding to Na^+/glucose cotransporters is determined by the carboxyl-terminal half of the protein. *J. Biol. Chem. 271*, 10029−10034.
3. Panayotova-Heiermann, M., Eskandari, S., Turk, E., Zampighi, G. A., and Wright, E. M. (1997) Five transmembrane helices form the sugar pathway through the Na^+/glucose cotransporter. *J. Biol. Chem. 272*, 20324−20327.
4. Turk E., and Wright, E. M. (1997) Membrane topology motifs in the SGLT cotransporter family. *J. Membr. Biol. 159*, 1−20.
5. Lo, B., and Silverman, M. (1998) Cysteine scanning mutagenesis of the segment between putative transmembrane helices IV and V of the high affinity Na^+/Glucose cotransporter SGLT1. Evidence that this region participates in the Na^+ and voltage dependence of the transporter. *J. Biol. Chem. 273*, 29341−29351.
6. Quick, M., Loo, D. D. F., and Wright, E. M. (2001) Neutralization of a conserved amino acid residue in the human Na^+/glucose cotransporter (hSGLT1) generates a glucose-gated H^+ channel. *J. Biol. Chem. 276*, 1728−1734.
7. Díez-Sampedro, A., Wright, E. M., and Hirayama, B. A. (2001) Residue 457 controls sugar binding and transport in the Na^+/glucose cotransporter. *J. Biol. Chem. 276*, 49188−49194.
8. Novakova, R., Homerova, D., Kinne, R. K. H., Kinne-Saffran, E., and Lin, J. T (2001) Identification of a region critically involved in the interaction of phlorizin with the rabbit sodium-D-glucose cotransporter SGLT1. *J. Membr. Biol. 184*, 55−60.
9. Meinild, A.-K., Loo, D. D. F., Hirayama, B. A., Gallardo, E., and Wright, E. M. (2001) Evidence for the involvement of Ala 166 in coupling Na^+ to sugar transport through the human Na^+/glucose cotransporter. *Biochemistry 40*, 11897−11904.
10. Parent, L., Supplisson, S., Loo, D. D. F., and Wright, E. M. (1992) Electrogenic properties of the cloned Na^+/glucose cotransporter: II. A transport model under nonrapid equilibrium conditions. *J. Membr. Biol. 125*, 63−79.
11. Ikeda, T. Y., Hwang, E.-S., Coady, M. J., Hirayama, B. A., Hediger, M. A., and Wright, E. M. (1989) Characterization of a Na^+/glucose cotransporter cloned from rabbit small intestine. *J. Membr. Biol. 110*, 87−95.
12. Loo, D. D. F., Hazama, A., Supplisson, S., Turk, E., and Wright, E. M. (1993) Relaxation kinetics of the Na^+/glucose cotransporter. *Proc. Natl. Acad. Sci. U.S.A. 90*, 5767−5771.
13. Mackenzie, G., Loo, D. D. F., and Wright, E. M. (1998) Relationships between Na^+/glucose cotransporter (SGLT1) currents and fluxes. *J. Membr. Biol. 162*, 101−106.
14. Díez-Sampedro, A., Eskandari, S., Wright, E. M., and Hirayama, B. A. (2001) Na^+-to-sugar stoichiometry of SGLT3. *Am. J. Physiol. Renal Physiol. 49*, F278−F282.
15. Meinild, A.-K., Hirayama, B. A., Wright, E. M., and Loo, D. D. F. (2002) Fluorescence studies of ligand-induced conformational changes of the Na^+/glucose cotransporter. *Biochemistry 41*, 1250−8.
16. Loo, D. D. F., Hirayama, B. A., Gallardo, E. M., Lam, J. T., and Turk, E., Wright, E. M. (1998) Conformational changes couple Na^+ and glucose transport. *Proc. Natl. Acad. Sci. U.S.A. 95*, 7789−7794.
17. Zampighi, G. A., Kerman, M., Boorer, K. J., Loo, D. D. F., Bezanilla, F., Chandy, G., Hall, J. E., and Wright, E. M. (1995) A method for determining the unitary functional capacity of cloned channels and transporters expressed in *Xenopus laevis* oocytes. *J. Membr. Biol. 148*, 65−78.
18. Restrepo, D., and Kimmich, G. A. (1985) Kinetic analysis of mechanism of intestinal Na^+-dependent sugar transport. *Am. J. Physiol. 248*, C498−C509.
19. Berteloot, A. (2003) Kinetic mechanism of Na^+-glucose cotransport through the rabbit intestinal SGLT1 protein. *J. Membr. Biol. 192*, 89−100.
20. Xie, Z., Turk, E., and Wright, E. M. (2000) Characterization of the *Vibrio parahaemolyticus* Na^+/glucose cotransporter. *J. Biol. Chem. 275*, 25959−25964.
21. Martin, M. G., Turk, E., Lostao, M. P., Kerner, C., and Wright, E. M. (1996) Defects in Na^+/glucose cotransporter (SGLT1) trafficking and function cause glucose-galactose malabsorption. *Nat. Genet. 12*, 216−220.
22. Hirayama, B. A., Loo, D. D. F, and Wright, E. M. (1997) Cation effects on protein conformation and transport in the Na^+/glucose cotransporter. *J. Biol. Chem. 272*, 2110−2115.
23. Díez-Sampedro, A., Hirayama, B. A., Osswald, C., Gorboulev, V., Baumgarten, K., Volk, C., Wright, E. M., and Koepsell, H. (2003) A glucose sensor hiding in a family of cotransporters. *Proc. Natl. Acad. Sci. U.S.A. 100*, 11753−11758.
24. Umbach, J., Coady, M. J., and Wright, E. M. (1990) Intestinal Na^+/glucose cotransporter expressed in *Xenopus* oocytes is electrogenic, *Biophys. J. 57*, 1218−1224.
25. Bissonnette, P., Noël, J., Coady, M. J., and Lapointe, J.-Y. (1999) Functional expression of tagged human Na^+-glucose cotransporter in *Xenopus laevis* oocytes. *J. Physiol. 520*, 359−371.
26. Borre, L., and Kanner, B. I. (2004) Arginine 445 controls the coupling between glutamate and cations in the neuronal transporter EAAC-1. *J. Biol. Chem. 279*, 2513−2519.
27. Bendahan, A., Armon, A., Madani, N., Kavanaugh, M. P., and Kanner, B. I. (2000) Arginine 447 plays a pivotal role in substrate interactions in a neuronal glutamate transporter. *J. Biol. Chem. 275*, 37436−37442.
28. Meredith, D. (2004) Site-directed mutation of arginine 282 to glutamate uncouples the movement of peptides and protons by the rabbit proton-peptide cotransporter PepT1. *J. Biol. Chem. 279*, 15795−15798.
29. Quick, M., Stölting, S., and Jung, H. (1999) Role of conserved Arg40 and Arg117 in the Na^+/proline transporter of *Escherichia coli*. *Biochemistry 38*, 13523−13529.

BI048652D